Original Paper

Joule heat calculations for simulations of multielectrode glass melters and in situ vitrification systems

Delbert L. Lessor, L. Loren Eyler and Patrick S. Lowery
Pacific Northwest Laboratory, Richland, WA (USA)

A procedure is developed for calculating Joule heating power density in simulating multielectrode, multiphase, generalized waveform electrically heated glass melters and in situ vitrification systems. A superposition principle valid at low frequencies allows calculating the cycle-averaged power density from a set of potential amplitude solutions, each solution having a current source amplitude in one electrode and a current sink amplitude in another electrode of a driven electrode pair. The calculated cycle-averaged power density can be coupled to balance equations for flow and energy in molten glass or soil. The procedure has advantages over the complex harmonic form for analyzing systems having waveforms chopped by silicon controlled rectifiers. A Scott-T transformer configuration with two emfs driving diagonally opposite electrodes in a rectangular array is one configuration having practical significance. Symmetries of this configuration are affected by amplitudes, phase relations, and waveforms of the electrical driving.

Berechnung der Jouleschen Wärme zur Simulation von Mehrelektroden-Glasschmelzwannen und von in situ Verglasungssystemen

Es wird ein Verfahren entwickelt, mit dem die Leistungsdichte der Jouleschen Aufheizung für die Simulation von elektrisch beheizten Mehrelektroden-, Mehrphasen-Glasschmelzwannen, bei generalisierter Wellenform, und von in situ Verglasungssystemen berechnet werden kann. Ein bei niedrigen Frequenzen gültiges Superpositionsprinzip ermöglicht die Berechnung der im geschlossenen Prozeß erzielten durchschnittlichen Leistungsdichte aus einer Folge von Spannungsamplitudenlösungen, wobei jede Lösung eine Stromquellenamplitude in der einen Elektrode und eine Stromsenkenamplitude in der anderen Elektrode eines angeschlossenen Elektrodenpaares besitzt. Die berechnete durchschnittliche Leistungsdichte eines geschlossenen Prozesses kann mit Bilanzgleichungen für die Strömung und die Energie in Glasschmelzen oder bei Verglasungen von kontaminierten Industrieabfällen verbunden werden. Das Verfahren hat Vorteile gegenüber der komplexharmonischen Methode, wenn Wellenformsysteme zu analysieren sind, die mit siliciumgesteuerten Gleichrichtern erzeugt werden. Eine Scott-T-Transformatorkonfiguration mit 2 EMKs, von diagonal gegenüberliegenden Elektroden versorgt, die rechtwinklig angeordnet sind, ist in der Praxis durchaus anwendbar. Symmetrien dieser Konfiguration werden durch Amplituden, Phasenbeziehungen und Wellenformen der elektrischen Versorgung beeinflußt.

1. Introduction

Materials in large volume, as in glass melters or in situ vitrification, can be heated by conduction of electric current. Optimizing transmission or distribution frequently requires multiphase, multielectrode configurations. Power control measures frequently lead to non-sinusoidal waveforms. Care is required in calculating power density distribution when Alternating Current (AC) power sources are used in which waveforms and phases differ in multiple electrode pairings. A model developed for this purpose is the primary subject of this paper. The calculation of the distribution of Joule heating is critical in in situ vitrification simulations, just as in those for production glass melters.

In situ vitrification is a process developed to immobilize or destroy contaminants in soil. The process involves melting soil in and around a region of contamination. Melting is accomplished by passing electric current through the soil, generating Joule heat. Once melting has been accomplished in the soil surrounding a contaminated region, the molten mass is allowed to cool. When cool, the vitrified material provides a stable, enduring encapsulation.

During the melting and cooling process, molten soil convects. The convection process is key to melt front progression which determines the encapsulated volume upon final cooling. Simulation of this process requires an understanding of the coupled flow, thermal, and electric processes. The coupled three-dimensional flow and melt volume can be investigated by numerical simulation of governing equations for the conservation of mass, momentum, energy, and electric charge in space and time. These methods also apply to Joule-heated production glass melter simulations.

The space-time factorization method calculates Joule heat power density for these simulations from reference steady-state current densities for each source-sink electrode pair operated separately. The Joule heat power density is a linear combination of inner products of these reference current densities multiplied by time-averaged products of total currents driving the separate electrode pairs.

Received June 11, 1990.

2. Background

Glass melting by electrical Joule (resistive) heating has been used for many years. Staněk [1] describes many aspects of electric glass melting processes in the commercial glass industry. Both all-electric and electric-boosted melters are used.

In early pioneering glass melter modeling work, Curran [2 and 3] utilized a two-dimensional vorticity-stream function formulation to represent the flow field. An early three-dimensional model approach using a vorticity-based approach was demonstrated by Chen and Goodson [4]. Several years of development have led to more generally applicable three-dimensional analysis tools.

Choudhary [5 and 6] presents a computer modeling approach for analyzing a glass melter with electric heating. The work solves for the steady-state density, momentum, energy, and electric fields through discrete approximation of the governing equations. Alternating current power sources are treated by assuming that the electrical driving force consists of harmonic real and imaginary parts. The resulting current density is modeled as

$$\underline{J} = -\sigma \nabla \phi = -\sigma \nabla \hat{\phi}\, e^{i\omega t}. \tag{1}$$

Power density is calculated as a function of position as

$$\dot{Q} = \underline{J} \cdot \underline{J}^* / (2\sigma) \tag{2}$$

where J is the complex current density and J^* is its complex conjugate. The numerical procedures used by Choudhary are based on primitive variables and finite-difference solution techniques.

Other recent glass melter modeling work includes that of Ungan and Viskanta [7], Ghandakly and Curran [8], and Tiwary et al. [9]. Horvath and Hilbig [10] present a model approach based on a combination of energy balance methods and discrete flow methods.

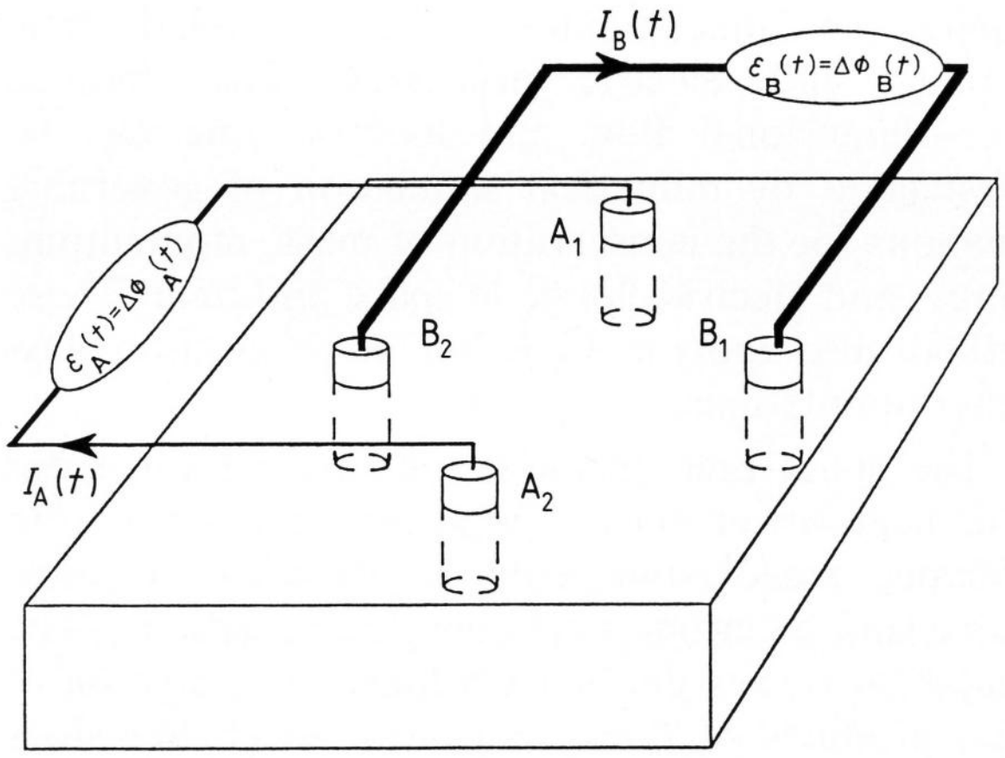

Figure 1. Four-electrode, two-phase in situ vitrification configuration.

Murnane et al. [11] present discussion and steady-state results of a finite-element model of the three-dimensional flows in glass melting processes. The FIDAP code was used. Several complex geometries of commercial glass melters are simulated, and predicted results of flow fields and particle transit paths are presented. Murnane et al. indicate that electrical potential field solutions were obtained for paired electrodes, as is done in the Joule heat calculation method described in this paper. Murnane et al. indicate that a root-mean-square (rms) voltage field was calculated and used in Joule heat computations, taking account of phase relations.

Glass melting using Joule heat has been extended to in situ vitrification [12 and 13]. The currently favored concept has two pairs of electrodes inserted into the soil in a rectangular array (figure 1). These are driven by AC power sources. Current passes between electrode pairs, dissipating energy in the soil as Joule heat. The Joule heat field has a spatial dependence determined by the current density and electrical conductivity fields. Electrical conductivity of the soil varies through several orders of magnitude in the region due to its strong temperature dependence. At elevated temperatures, soils become molten and convection is induced by buoyancy forces. Melt front progression is governed in part by convective heat flow processes.

The method for calculating Joule heating power density reported in this paper can be coupled to many of the previous simulation formulations, in either primitive variable or stream function form, and using either finite elements or finite differences. The essential code features needed are the ability to calculate electrical potential in a region having current sources and sinks, and a volumetric heating term in the energy equation. The present method allows a broad class of time dependencies of the driving voltages or currents, in contrast to the exp ($i\omega t$) form used by Choudhary [5 and 6]. It is more rigorously correct than the rms voltage field method of Murnane et al. [11]. It also allows altering the calculated heating distribution due to a change in the electrical driving without recalculating spatial fields; a field recalculation is necessary only when the electrical conductivity distribution changes.

3. Conservation and balance equations

The primitive variable approach to the numerical solution of the governing conservation equations provides many advantages over the vorticity-stream function approach. Efficient solution algorithms have been developed, specification of boundary conditions is straightforward, and extensive applicability has been shown to a wide range of coupled thermal hydraulic problems. This technique solves discrete approximations for the mass, momentum, energy, charge and constituent conservation equations in

primitive variable form, e.g., density, velocity, and temperature. Finite-difference and finite-element techniques are the principal basis for numerical approximations in use in coupled melter flow and thermal analysis. Finite-difference methods have been employed in the TEMPEST family of codes [14 and 15], one version of which includes fully coupled electric field solution for obtaining position and time dependence of resistance heating (Joule heat) in a glass melt [16].

The mathematical equations solved in TEMPEST are as follows (Einsteinian tensor notation and convention is used):

conservation of mass

$$\frac{\partial U_j}{\partial X_j} = 0\,; \tag{3}$$

conservation of momentum

$$\frac{\partial U_i}{\partial t} + \frac{\partial U_j U_i}{\partial X_j} = -\frac{1}{\varrho_0}\frac{\partial p}{\partial X_i} + \frac{\varrho}{\varrho_0} g_i + \frac{\partial}{\partial X_j}\left(\nu \frac{\partial U_i}{\partial X_j}\right) + \left(\frac{\partial \nu}{\partial X_j}\right)\left(\frac{\partial U_j}{\partial X_i}\right); \tag{4}$$

conservation of energy

$$\varrho\, C \left(\frac{\partial T}{\partial t} + \frac{\partial U_j T}{\partial X_j}\right) = \frac{\partial}{\partial X_j}\left(k \frac{\partial T}{\partial X_j}\right) + \dot{Q}\,. \tag{5}$$

Here X_j and U_j are the j-th position and velocity components, respectively; ϱ and ϱ_0 are local and reference mass density, respectively (used in the Boussinesq approximation); p is pressure; g_i is the i-th component of the gravitational acceleration; T is temperature; C is heat capacity; k is thermal conductivity; and $\dot{Q}$ is rate of heat generation per unit volume.

Finite-difference techniques are used in TEMPEST to approximate these equations. The fluid region is assumed incompressible and the Boussinesq approximation has been used in formulating equations (3 to 5). The time scales for velocity and temperature changes are typically longer than an electrical cycle. Therefore, it is acceptable to replace the instantaneous volumetric heat generation rate $\dot{Q}$ by its cycle average.

The method presented here for cycle-averaged heat generation per unit volume can be coupled to any set of determining mass, momentum, and energy balance equations comparable to equations (3 to 5), whether solved in finite difference, finite element, or other form.

4. Electric model

For multielectrode, multiphase electrical driving, a superposition principle for potential allows calculation of the cycle- averaged Joule heat per unit volume from sets of time-independent potential solutions and the mean squares and mean products of the currents or voltages. The waveforms need not be sinusoidal for this analysis to be valid. Hence, Silicon-Controlled Rectifier (SCR) chopping of the waveform can be modeled.

The in situ vitrification concept with a square array of electrodes and two-phase voltage driving can be modeled by techniques which will be described. Each pair of diagonally opposed electrodes is driven by an approximately sinusoidal voltage source (figure 1). The phases for the two diagonal electromotive forces (emfs) differ by approximately 90°, however. Theory and procedure will here be presented for calculating Joule heating from this electrode configuration in an in situ vitrification simulation using TEMPEST. Generality is maintained whenever convenient. In particular, the authors will specialize to the square array of electrodes and 90°-phase differences only in discussing reduction of the modeling region by using symmetry. Further, somewhat arbitrary voltage and current waveforms will be considered rather than purely sinusoidal ones.

The conservation of electrical charge implies that

$$\frac{\partial \varrho_e}{\partial t} + \nabla \cdot \underline{J} = Q_v \tag{6}$$

where ϱ_e is electric charge density, $\underline{J}$ is electric current density, and Q_v is charge produced per unit volume per unit time. Because charge is conserved, Q_v is actually zero, but a nonzero Q_v is useful to represent the introduction of current into a modeled region by processes not modeled. If field change with time is sufficiently slow, the accumulation and dissipation of volumetric and surface charge can be neglected, and the term $\partial \varrho_e / \partial t$ can be neglected to give

$$\nabla \cdot \underline{J} = Q_v\,. \tag{7}$$

The condition for this neglect of capacitive (charge storage) effects is

$$\Delta t \gg \varepsilon/\sigma \tag{8}$$

or in terms of the frequency, ω, of significantly represented Fourier components

$$\varepsilon\, \omega/\sigma \ll 1 \tag{9}$$

where Δt is the amount of time over which driving conditions (voltage or current sources) vary significantly, ε is electrical permittivity, and σ is electrical conductivity. Capacitive effects are negligible if conditions (8 and 9) hold at all points along at least one sufficiently wide path leading from each electrode to each other electrode through the region of

interest. This is equivalent to the negative voltage gradient and local current density being in phase.

Suppose that a modeling region is driven with two possible current source-sink systems, $Q_A(\underline{r}, t)$ or $Q_B(\underline{r}, t)$, in the region interior. Each current source distribution will have an associated potential distribution, ϕ_A and ϕ_B, determined by it and the boundary conditions

$$\nabla \cdot (-\sigma \nabla \phi_A) = Q_A \,, \qquad \nabla \cdot (-\sigma \nabla \phi_B) = Q_B \,. \tag{10}$$

ϕ has been written as the electrical potential, and Ohm's law has been assumed:

$$\underline{J} = \sigma \underline{E} = -\sigma \nabla \phi \,. \tag{11}$$

It is assumed that Lorentz force effects are small in determining the current distribution, an assumption justified by Staněk [1].

Due to the linearity of the governing equations, if $\phi_A(\underline{r}, t)$ and $\phi_B(\underline{r}, t)$ are solutions to equation (10) on the interior of a modeling region with current sources $Q_A(\underline{r}, t)$ and $Q_B(\underline{r}, t)$, respectively, then $\phi_A(\underline{r}, t) + \phi_B(\underline{r}, t)$ is a solution on the interior of that region with current source $Q_A(\underline{r}, t) + Q_B(\underline{r}, t)$ applied:

$$\nabla \cdot (-\sigma \nabla (\phi_A + \phi_B)) = Q_A + Q_B \,. \tag{12}$$

If the boundary of the region is everywhere insulated, then the condition at positions $\underline{r}$ on the boundary is that of zero normal current density:

$$J_{n,A}(\underline{r}, t) = \hat{n} \cdot (-\sigma \nabla \phi_A) = 0 \,, \qquad J_{n,B}(\underline{r}, t) = \hat{n} \cdot (-\sigma \nabla \phi_B) = 0 \,. \tag{13}$$

If ϕ_A and ϕ_B satisfy this insulating boundary condition, then $\phi_A + \phi_B$ will satisfy it also. The result is that, for an insulated region with interior current sources, the potential distribution when two sets of current sources $Q_A(\underline{r}, t)$ and $Q_B(\underline{r}, t)$ operate is the sum $\phi_A(\underline{r}, t) + \phi_B(\underline{r}, t)$ of the associated potential distributions with a possible additive function of t alone:

$$\phi_{A \text{ and } B}(\underline{r}, t) = \phi_A(\underline{r}, t) + \phi_B(\underline{r}, t) + \Psi(t) \,. \tag{14}$$

It is noted, of course, that each current source distribution must sum to zero over the modeling region for consistency with the insulating boundary conditions:

$$\int Q_A(\underline{r}, t)\, d^3 r = 0 \,, \qquad \int Q_B(\underline{r}, t)\, d^3 r = 0 \,. \tag{15}$$

If part of the boundary is grounded and the remainder insulated, equation (14) still applies, with $\Psi(t)$ identically zero.

Now cases are considered in which each current source distribution has the same time dependence throughout the modeling region, with major changes occurring only over time periods much longer than ε/σ. The source terms in this case can be separated into spatial and time varying factors as

$$Q_A(\underline{r}, t) = Q_A^{(0)}(\underline{r})\, f_A(t) \,, \qquad Q_B(\underline{r}, t) = Q_B^{(0)}(\underline{r})\, f_B(t) \,. \tag{16}$$

With this assumption, the potentials for the cases of one source set operating can be similarly factored:

$$\phi_A(\underline{r}, t) = \phi_A^{(0)}(\underline{r})\, f_A(t) \,, \qquad \phi_B(\underline{r}, t) = \phi_B^{(0)}(\underline{r})\, f_B(t) \,. \tag{17}$$

Equation (17) permits the tremendous simplification of allowing time-independent Poisson equations to determine the spatial dependence of the electrical potential over an extended period of time:

$$\nabla \cdot (-\sigma \nabla \phi_A^{(0)}(\underline{r})) = Q_A^{(0)}(\underline{r}) \,, \qquad \nabla \cdot (-\sigma \nabla \phi_B^{(0)}(\underline{r})) = Q_B^{(0)}(\underline{r}) \,. \tag{18}$$

The potential amplitude solutions (equation 18) and the time dependencies from equations (16 and 17) describe the melt region until electrical conductivity $\sigma(\underline{r})$ changes significantly.

It is assumed that the current source sets $Q_A^{(0)}(\underline{r})$ (or $Q_B^{(0)}(\underline{r})$) have one region of positive injection of current into the modeling region, and call that region A_1 (or B_1), with A_2 (or B_2) being the corresponding sink region. It is assumed further that the regions of current injection or withdrawal are electrodes of sufficiently high electrical conductivity that each is essentially an equipotential volume. The reference current amplitude $I_A^{(0)}$ is a measure of the source strength:

$$I_A^{(0)} = \int_{A_1} Q_A^{(0)}(\underline{r})\, d^3 r = -\int_{A_2} Q_A^{(0)}(\underline{r})\, d^3 r \,. \tag{19}$$

The integrations are over the volume of the source (A_1) and sink (A_2). The instantaneous electric currents flowing into the modeling region at A_1 and B_1 are $I_A(t) = I_A^{(0)} f_A(t)$ and $I_B(t) = I_B^{(0)} f_B(t)$, respectively. In a simulation for a melt region with two electrode pairs, $I_A^{(0)}$ and $I_B^{(0)}$ can be set to convenient values. Equation (18) is then solved for the reference potential distributions $\phi_A^{(0)}(\underline{r})$ and $\phi_B^{(0)}(\underline{r})$. Time-dependent linear combinations of these reference potential distributions are used for the case of both A

and B sources operating, first to match measured or desired global parameters (total powers, voltages, or currents), then to calculate the local Joule heating power per unit volume, using the procedure which will be described.

The six time-averaged global quantities $\overline{P}_A$, $\overline{P}_B$, $I_{A,\,rms}$, $I_{B,\,rms}$, $\Delta\phi_{A,\,rms}$, and $\Delta\phi_{B,\,rms}$ for fixed geometry, fixed conductivity, and fixed $I_A^{(0)}$ and $I_B^{(0)}$, depend only on the three quantities

$$F_{AA} = 1/T \int_0^T f_A^2(t)\,dt\,, \tag{20}$$

$$F_{BB} = 1/T \int_0^T f_B^2(t)\,dt\,, \tag{21}$$

$$F_{AB} = 1/T \int_0^T f_A(t)\,f_B(t)\,dt\,. \tag{22}$$

$\overline{P}_A$, $I_{A,\,rms}$, and $\Delta\phi_{A,\,rms}$ are the average power supplied by the emf source to electrode pair A, the rms current from the A emf source, and the rms voltage across the A electrode pair, respectively. Similar definitions apply for the B electrode pair. The time-averaged global quantities are sensitive to details of the current waveforms only through the three parameters F_{AA}, F_{BB}, and F_{AB}, subject to the constraint of equations (8 or 9). In the calculation of the thermal transient, the local Joule heating power density must be calculated. If significant temperature changes occur only over many electrical cycles, only the time-averaged local Joule heating power is needed. The instantaneous local Joule heating power per unit volume is

$$\begin{aligned} P_v &= \underline{J} \cdot \underline{E} = \sigma\,(\nabla\,\phi)^2 = \\ &= \sigma\,[f_A(t)\,\nabla\,\phi_A^{(0)}(\underline{r}) + f_B(t)\,\nabla\,\phi_B^{(0)}(\underline{r})]^2\,. \end{aligned} \tag{23}$$

This gives a time-averaged power per unit volume $\overline{P}_v$:

$$\begin{aligned} \overline{P}_v = {} & F_{AA}\,\sigma\,[\nabla\,\phi_A^{(0)}]^2 + F_{BB}\,\sigma\,[\nabla\,\phi_B^{(0)}]^2 + \\ & + 2\,F_{AB}\,\sigma\,[\nabla\,\phi_A^{(0)} \cdot \nabla\,\phi_B^{(0)}]\,. \end{aligned} \tag{24}$$

Thus, $\overline{P}_v$ depends on F_{AA}, F_{BB}, and F_{AB}, and not on other details of the waveforms.

5. Model implementation

To calculate the time- und position-dependent currents, potentials, and fields, quantities required from the potential amplitude solutions are

$$I_A^{(0)},\ \phi_A^{(0)}(\underline{r}_{A1}) - \phi_A^{(0)}(\underline{r}_{A2}),\ \phi_A^{(0)}(\underline{r}_{B1}) - \phi_A^{(0)}(\underline{r}_{B2}),\ \phi_A^{(0)}(\underline{r}),\ -\nabla\,\phi_A^{(0)}(\underline{r}) \tag{25}$$

and

$$I_B^{(0)},\ \phi_B^{(0)}(\underline{r}_{B1}) - \phi_B^{(0)}(\underline{r}_{B2}),\ \phi_B^{(0)}(\underline{r}_{A1}) - \phi_B^{(0)}(\underline{r}_{A2}),\ \phi_B^{(0)}(\underline{r}),\ -\nabla\,\phi_B^{(0)}(\underline{r})\,. \tag{26}$$

The instantaneous quantities are combinations of these reference quantities or their products multiplied by $f_A(t)$ and/or $f_B(t)$, or products thereof. It is necessary only to determine the quantities F_{AA}, F_{BB}, and F_{AB} for each time step in a transient calculation in order to calculate the local cycle-averaged Joule heating from equation (24).

The related time-averaged global parameters are

$$\overline{P}_A = I_A^{(0)}\,[\phi_A^{(0)}(\underline{r}_{A1}) - \phi_A^{(0)}(\underline{r}_{A2})]\,F_{AA} + I_A^{(0)}\,[\phi_B^{(0)}(\underline{r}_{A1}) - \phi_B^{(0)}(\underline{r}_{A2})]\,F_{AB}\,; \tag{27}$$

$$\overline{P}_B = I_B^{(0)}\,[\phi_B^{(0)}(\underline{r}_{B1}) - \phi_B^{(0)}(\underline{r}_{B2})]\,F_{BB} + I_B^{(0)}\,[\phi_A^{(0)}(\underline{r}_{B1}) - \phi_A^{(0)}(\underline{r}_{B2})]\,F_{AB}\,; \tag{28}$$

$$I_{A,\,rms} = I_A^{(0)}\,(F_{AA})^{1/2}, \tag{29}$$

$$I_{B,\,rms} = I_B^{(0)}\,(F_{BB})^{1/2}; \tag{30}$$

$$\begin{aligned} \Delta\phi_{A,\,rms} = {} & \{[\phi_A^{(0)}(\underline{r}_{A1}) - \phi_A^{(0)}(\underline{r}_{A2})]^2\,F_{AA} + [\phi_B^{(0)}(\underline{r}_{A1}) - \phi_B^{(0)}(\underline{r}_{A2})]^2\,F_{BB} + \\ & + 2\,[\phi_A^{(0)}(\underline{r}_{A1}) - \phi_A^{(0)}(\underline{r}_{A2})]\,[\phi_B^{(0)}(\underline{r}_{A1}) - \phi_B^{(0)}(\underline{r}_{A2})]\,F_{AB}\}^{1/2}\,; \end{aligned} \tag{31}$$

$$\begin{aligned} \Delta\phi_{B,\,rms} = {} & \{[\phi_A^{(0)}(\underline{r}_{B1}) - \phi_A^{(0)}(\underline{r}_{B2})]^2\,F_{AA} + [\phi_B^{(0)}(\underline{r}_{B1}) - \phi_B^{(0)}(\underline{r}_{B2})]^2\,F_{BB} + \\ & + 2\,[\phi_A^{(0)}(\underline{r}_{B1}) - \phi_A^{(0)}(\underline{r}_{B2})]\,[\phi_B^{(0)}(\underline{r}_{B1}) - \phi_B^{(0)}(\underline{r}_{B2})]\,F_{AB}\}^{1/2}. \end{aligned} \tag{32}$$

The global parameters (equations 27 to 32) have been expressed in terms of F_{AA}, F_{BB}, and F_{AB}, which are properties of the current waveforms in circuits A and B. With the aid of reference solutions $\phi_A^{(0)}(\underline{r})$ and $\phi_B^{(0)}(\underline{r})$, the voltage waveform information can be used to deduce the current waveform information.

The instantaneous voltage difference across electrode pairs can be written as

$$\Delta\phi_A(t) = f_A(t)\,\Delta\phi^{(0)}_{A,A} + f_B(t)\,\Delta\phi^{(0)}_{B,A}\,,$$
$$\Delta\phi_B(t) = f_A(t)\,\Delta\phi^{(0)}_{A,B} + f_B(t)\,\Delta\phi^{(0)}_{B,B} \qquad (33)$$

where

$$\Delta\phi_A(t) = \phi(\underline{r}_{A1}, t) - \phi(\underline{r}_{A2}, t)\,,$$
$$\Delta\phi^{(0)}_{A,A} = \phi^{(0)}_A(\underline{r}_{A1}) - \phi^{(0)}_A(\underline{r}_{A2})\,, \qquad (34)$$
$$\Delta\phi^{(0)}_{A,B} = \phi^{(0)}_A(\underline{r}_{B1}) - \phi^{(0)}_A(\underline{r}_{B2}),\ \text{etc.}$$

Equation (33) can be inverted to express the current waveforms $f_A(t)$ and $f_B(t)$ in terms of the voltage difference waveforms $\Delta\phi_A(t)$ and $\Delta\phi_B(t)$. One obtains

$$f_A(t) = \frac{\Delta\phi^{(0)}_{B,B}}{D}\,\Delta\phi_A(t) - \frac{\Delta\phi^{(0)}_{B,A}}{D}\,\Delta\phi_B(t)\,, \qquad (35)$$
$$f_B(t) = \frac{\Delta\phi^{(0)}_{A,A}}{D}\,\Delta\phi_B(t) - \frac{\Delta\phi^{(0)}_{A,B}}{D}\,\Delta\phi_A(t)$$

where

$$D = \Delta\phi^{(0)}_{A,A}\,\Delta\phi^{(0)}_{B,B} - \Delta\phi^{(0)}_{A,B}\,\Delta\phi^{(0)}_{B,A}\,. \qquad (36)$$

Equations (35 and 20 to 22) yield

$$F_{AA} = \left(\frac{\Delta\phi^{(0)}_{B,B}}{D}\right)^2 G_{AA} + \left(\frac{\Delta\phi^{(0)}_{B,A}}{D}\right)^2 G_{BB} - 2\,\frac{\Delta\phi^{(0)}_{B,B}\,\Delta\phi^{(0)}_{B,A}}{D^2}\,G_{AB}\,, \qquad (37)$$

$$F_{BB} = \left(\frac{\Delta\phi^{(0)}_{A,A}}{D}\right)^2 G_{BB} + \left(\frac{\Delta\phi^{(0)}_{A,B}}{D}\right)^2 G_{AA} - 2\,\frac{\Delta\phi^{(0)}_{A,A}\,\Delta\phi^{(0)}_{A,B}}{D^2}\,G_{AB}\,, \qquad (38)$$

$$F_{AB} = \{-\Delta\phi^{(0)}_{B,B}\,\Delta\phi^{(0)}_{A,B}\,G_{AA} - \Delta\phi^{(0)}_{B,A}\,\Delta\phi^{(0)}_{A,A}\,G_{BB} + [\Delta\phi^{(0)}_{A,A}\,\Delta\phi^{(0)}_{B,B} + \Delta\phi^{(0)}_{B,A}\,\Delta\phi^{(0)}_{A,B}]\,G_{AB}\}/D^2 \qquad (39)$$

where

$$G_{AA} = 1/T\int_0^T [\Delta\phi_A(t)]^2\,\mathrm{d}t\,, \qquad (40)$$

$$G_{BB} = 1/T\int_0^T [\Delta\phi_B(t)]^2\,\mathrm{d}t\,, \qquad (41)$$

$$G_{AB} = 1/T\int_0^T [\Delta\phi_A(t)\,\Delta\phi_B(t)]\,\mathrm{d}t\,. \qquad (42)$$

In terms of the G parameters (instead of the F parameters) it reads:

$$\Delta\phi_{A,\,\mathrm{rms}} = (G_{AA})^{1/2}\,, \qquad (43)$$

$$\Delta\phi_{B,\,\mathrm{rms}} = (G_{BB})^{1/2}\,; \qquad (44)$$

$$\overline{P}_A = I^{(0)}_A\left[\frac{\Delta\phi^{(0)}_{B,B}}{D}\,G_{AA} - \frac{\Delta\phi^{(0)}_{B,A}}{D}\,G_{AB}\right], \qquad (45)$$

$$\overline{P}_B = I^{(0)}_B\left[\frac{\Delta\phi^{(0)}_{A,A}}{D}\,G_{BB} - \frac{\Delta\phi^{(0)}_{A,B}}{D}\,G_{AB}\right]; \qquad (46)$$

$$I_{A,\,\mathrm{rms}} = I^{(0)}_A\left\{\left[\frac{\Delta\phi^{(0)}_{B,B}}{D}\right]^2 G_{AA} + \left[\frac{\Delta\phi^{(0)}_{B,A}}{D}\right]^2 G_{BB} - 2\,\frac{\Delta\phi^{(0)}_{B,B}\,\Delta\phi^{(0)}_{B,A}}{D^2}\,G_{AB}\right\}^{1/2}, \qquad (47)$$

$$I_{B,\,\mathrm{rms}} = I^{(0)}_B\left\{\left[\frac{\Delta\phi^{(0)}_{A,A}}{D}\right]^2 G_{BB} + \left[\frac{\Delta\phi^{(0)}_{A,B}}{D}\right]^2 G_{AA} - 2\,\frac{\Delta\phi^{(0)}_{A,A}\,\Delta\phi^{(0)}_{A,B}}{D^2}\,G_{AB}\right\}^{1/2}. \qquad (48)$$

At most, only three of the global parameters can be matched by choice of F_{AA}, F_{BB}, and F_{AB} (or G_{AA}, G_{BB}, and G_{AB}). Several options have been coded in the electric field version of TEMPEST for application to in situ vitrification:

a) Specify a consistent set of three of the six global parameters (equations 27 to 32), and ask the code to deduce F_{AA}, F_{BB}, and F_{AB} from them at each recalculation of the reference potential distribution or when driving emfs are changed.

b) Specify that the source currents are temporarily orthogonal (at $\pm$ 90° phase difference in the case of pure sinusoidal currents) and, hence, that $F_{AB} = 0$. Then specify matching of one of the following sets of two global parameters:
$(\overline{P}_A, \overline{P}_B)$, $(I_{B,\,\mathrm{rms}}, I_{A,\,\mathrm{rms}})$, $(\Delta\phi_{A,\,\mathrm{rms}}, \Delta\phi_{B,\,\mathrm{rms}})$, or some other admissible pair.

Note that $F_{AB} = 0$ occurs if the source current phases differ by $\pm$ 90° for purely sinusoidal waveforms, because

$$\int_0^{2\pi/\omega} \cos(\omega t + c)\cos(\omega t + c \pm \pi/2)\,\mathrm{d}t = 0$$

for any phase c.

c) Specify that the source voltages are orthogonal to

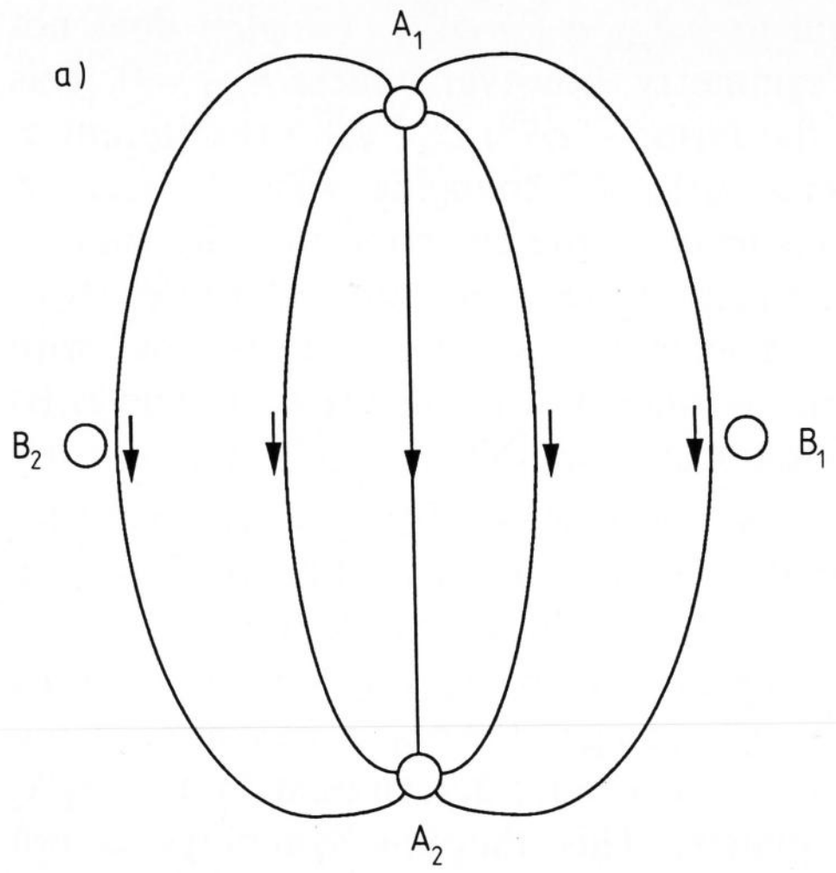

Figures 2a and b. Schematic current flow lines with a) only A electrodes driven, b) only B electrodes driven.

each other (their phases differ by $\pm 90°$ for pure sinusoidal emfs) and hence that $G_{AB} = 0$. Then specify matching of two of the global parameters.

d) Specify the set (F_{AA}, F_{BB}, F_{AB}) or the set (G_{AA}, G_{BB}, G_{AB}).

It is shown in section 4. that calculation of the average Joule heating power density requires only the two spatial solutions $\phi_A^{(0)}(\underline{r})$ and $\phi_B^{(0)}(\underline{r})$ of equation (18), one with the A electrodes driven by a constant current source, and one with the B electrodes driven (together with the time-averaged information in F_{AA}, F_{BB}, and F_{AB}). This model for Joule heating can be used in simulations using a three-dimensional heat and fluid flow solver with the following procedure:

– Model a region such that the boundary surfaces can be treated as either electrically insulating or held at zero potential.

– For a temperature distribution, calculate the spatial dependence of electrical conductivity σ.

– For each electrode pair separately, calculate a

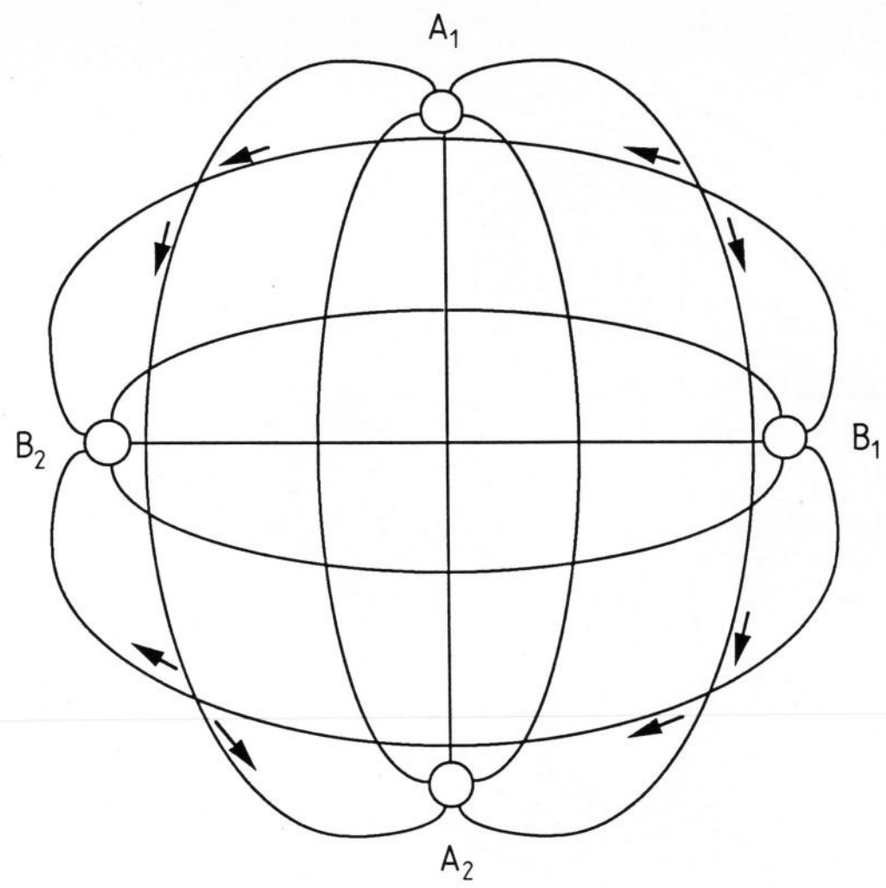

Figure 3. Lines of $-\nabla \phi_A^{(0)}$ and $-\nabla \phi_B^{(0)}$.

reference potential solution. For pair A, set source currents summing to $I_A^{(0)}$ in electrode A_1 and sink currents summing to $-I_A^{(0)}$ in electrode A_2. Then calculate the reference potential distribution $\phi_A^{(0)}(\underline{r})$. Do the same for the B set of electrodes.

– Set values of parameters F_{AA}, F_{BB}, and $\underline{F}_{AB}$ from a desired and determining subset of $\overline{P}_A$, $\overline{P}_B$, $I_{A,\,rms}$, $I_{B,\,rms}$, $\Delta\phi_{A,\,rms}$, and $\Delta\phi_{B,\,rms}$, and the reference solutions using equations (27 to 32) or equations (43 to 48 and 37 to 39).

– Calculate the position-dependent heat source $\overline{P}_v$ using equation (24) and the reference solutions $\phi_A^{(0)}(\underline{r})$ and $\phi_B^{(0)}(\underline{r})$.

– Calculate evolution of temperature distribution and flow fields from equations (3 to 5) or equivalent, using $\overline{P}_v$ as $\dot{Q}$ in equation (5).

– Repeat the second through the sixth step in the simulation when σ has changed or when the driving emfs are changed.

In this procedure, the change in electrical conductivity (which can vary through orders of magnitude in the modeled region) determines when new electrical potential solutions are needed.

6. Symmetry considerations

Reductions in the size of the modeling region for this calculation permitted by symmetry will here be considered, specializing to a rectangular array of electrodes as used in the in situ vitrification concept of Buelt et al. [13]. This concept uses a Scott-T transformer configuration for two emf sources. The electrode configuration of figure 1 will be assumed to have initially two planes of reflective symmetry, one through the A_1A_2 electrodes, and one through the B_1B_2 electrodes. This requires, of course, that the electrical conductivity initially has this same symmetry.

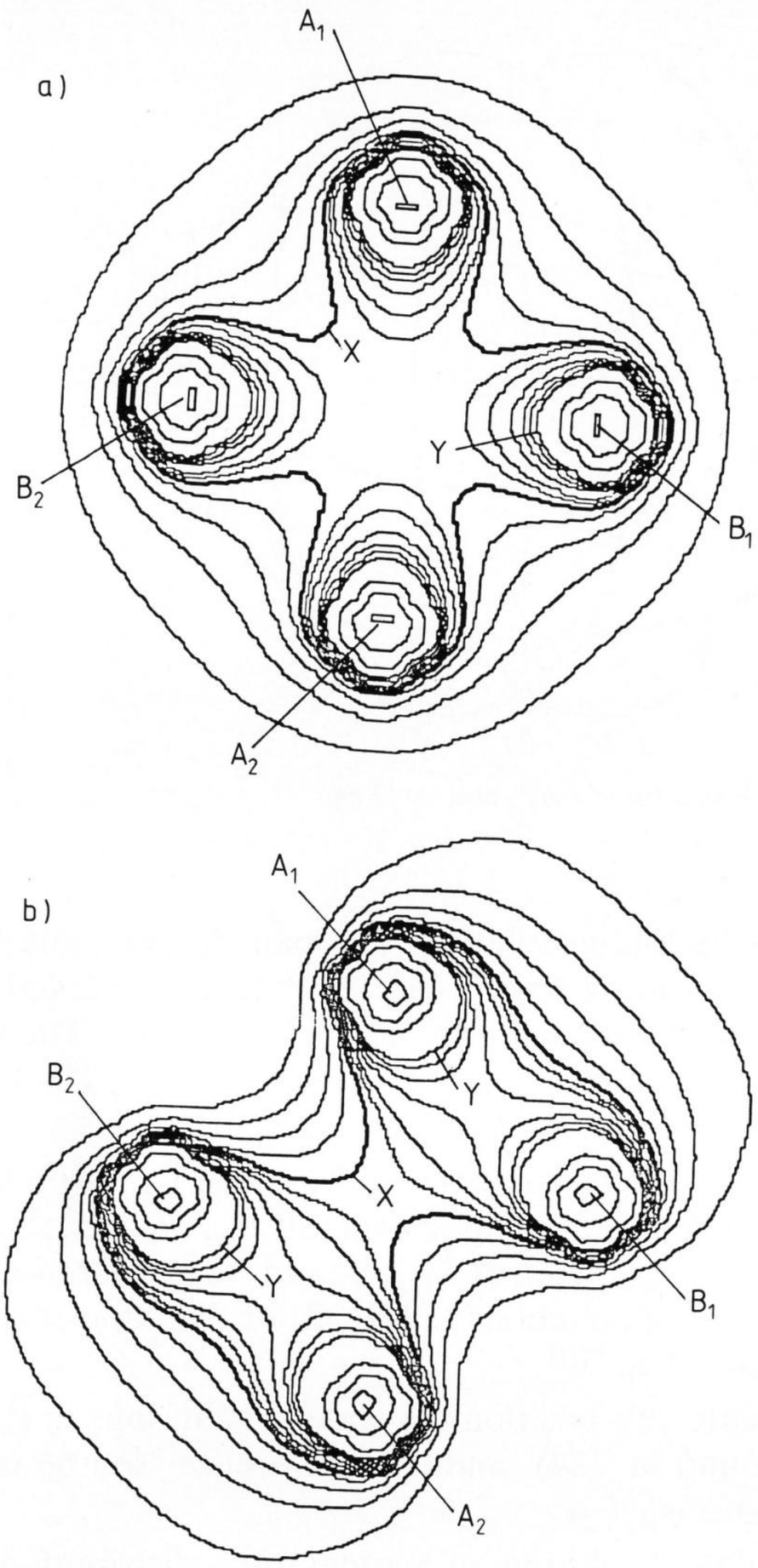

Figures 4a and b. Joule heat contours for a four-electrode, two-phase in situ vitrification configuration with a) $F_{AB} = 0$, b) $F_{AB} = -1$.

If the current was driven for a period of time through the A set alone or through the B set alone, the thermal symmetry about the A_1A_2 plane or the B_1B_2 plane would be preserved. The symmetry about planes at $\pm$ 45° to the A_1A_2 or B_1B_2 planes would be lost because of asymmetric heating, however. This is shown schematically in figures 2a and b, where lines of $-\nabla \phi_A^{(0)}$ and $-\nabla \phi_B^{(0)}$ are shown. The thermal symmetry is preserved with respect to reflection planes A_1A_2 or B_1B_2 in figure 2a or b if the current density vectors have the same magnitude at image points, even though they differ in inclination to the axes. This is because the Joule heat power density depends only on $\sigma (\nabla \phi)^2$.

Now consider the case in which both the A and B electrode pairs are driven, though with different time dependence. This is shown schematically in figure 3. The terms in $\overline{P}_v$ proportional to $F_{AA}\, \sigma\, (\nabla \phi_A^{(0)})^2$ and $F_{BB}\, \sigma\, (\nabla \phi_B^{(0)})^2$ retain symmetry. The term in $\overline{P}_v$ proportional to $2\, F_{AB}\, \sigma\, (\nabla \phi_A^{(0)}) \cdot (\nabla \phi_B^{(0)})$ does not retain this symmetry, however, unless $F_{AB} = 0$. This is because the term $(\nabla \phi_A^{(0)}) \cdot (\nabla \phi_B^{(0)})$ is different at image points, actually changing sign as seen in figure 3. This leads to the assertion that the analysis of the physically symmetric four-electrode, two-phase, in situ vitrification can be carried out with quarter-plane symmetry with planes A_1A_2 and B_1B_2 cutting the quarter planes if and only if $F_{AB} = 0$.

A carefully constructed diagram will indicate, however, that for the special case of equal amplitude driving of the A and B electrode pairs, thermal quarter-plane symmetry is again achieved, even for nonzero F_{AB} but having as the planes of symmetry the bisectors of the quadrants determined by the A_1A_2 and B_1B_2 planes. This thermal symmetry is not particularly useful in reducing the domain for electric potential calculations, however.

7. Joule heating calculation examples

Results of two sample calculations of Joule heat density will be presented using the potential gradients or current densities from a pair of reference time-independent potential solutions. Each reference potential solution has a current source in one electrode of a pair and a current sink at the other, as in the preceding theory. The effects of the temporal correlation "interference term" in the Joule heating will be illustrated. Differing Joule heat distributions calculable from the same pair of time-independent potential solutions with different temporal correlations (including different phase angles for purely harmonic driving) will be shown.

Figures 4a and b show the Joule heat contours for two different modes of driving a square array of diagonally opposed electrode pairs in a two-dimensional configuration. Define the top and bottom electrodes as A_1 and A_2, respectively, and the left and right electrodes as B_2 and B_1, respectively, in the notation of sections 4. to 6. The same set of Joule heat contour values has been plotted in figures 4a and b. Two of these levels (labeled X and Y in the figures) have been called out to illustrate spatial effects in the Joule heat field caused by the contribution of the "interference term" in the Joule heat computation.

In figure 4a, the electrode pairs were driven with equal rms currents and a temporal correlation factor $F_{AB} = 0$. This would include purely harmonic driving with equal amplitude currents and a relative phase of $\pm$ 90° as one case for which the results apply. Figure 4a shows that anticipated symmetries in the Joule heating are preserved. The Joule heat density at each position is, for the $F_{AB} = 0$ case, simply the sum of the Joule heat densities for each pair driven separately with the same rms current.

Figure 4b describes the case of equal rms current values in the two electrode pairs and a temporal correlation factor $F_{AB} = -1$. An increase in Joule heat density can be seen in quadrants 1 and 3 (taking figure center as origin and the line to the right as the positive X axis), where $\nabla \phi_A^{(0)} \cdot \nabla \phi_B^{(0)}$ is positive. A corresponding reduction in Joule heat density occurs in quadrants 2 and 4. The Joule heat power density shows symmetry about the quadrant bisectors. The case $F_{AB} = +1$ would interchange the quadrants having increased and reduced heating as compared with the $F_{AB} = -1$ case. The case $F_{AB} = 0$ is representative of Scott-T electrical driving; the $F_{AB} = \pm 1$ cases are not.

Although temporal correlation in the electrical driving has some effect on the Joule heat distribution for the square electrode array of figures 4a and b, the comparative insensitivity is the result of the near-orthogonality in space of the field lines in the two reference potential solutions throughout much of the modeled region.

Figures 5a to c show the Joule heat contours in a near-rectangular two-dimensional modeled region having electrode pairs A_1 (upper left) and A_2 (upper right) driven by current source A, and pair B_1 (lower left) and B_2 (lower right) driven by current source B. A slight "trough" extends the modeled region downward from the predominantly rectangular outline in the region between electrodes. Boundaries are electrically insulating. Electrodes are indicated in the figure. As was done for the contour plots of figures 4a and b, the same set of contour levels was plotted in each of figures 5a to c. Also as before, two contour levels have been called out in these figures (denoted as X and Y) to illustrate the effect of the "interference term" in the Joule heat computation.

Figure 5a shows the Joule heat contours for equal rms currents with temporal correlation $F_{AB} = 0$. The Joule heat power density is highest in the region near electrode edges, particularly edges near another electrode. Figure 5b shows the contours for the case $F_{AB} = 1$. Greater uniformity in heating is achieved with $F_{AB} = 1$, as this is thermally equivalent to driving the left electrodes together and the right electrodes together, filling much of the rectangle with nearly uniform, nearly parallel current. Driving with $F_{AB} = -1$, as shown in figure 5c, gives highest heating in the region between and near electrodes on the left and on the right of the modeled region and very low heating near the center of the modeled region.

The Joule heat distributions in the cases shown in figures 5a to c are very sensitive to the temporal correlation factor F_{AB}. This stems from the near-parallel orientation of $\nabla \phi_A^{(0)}$ and $\nabla \phi_B^{(0)}$ in much of the modeled region.

In considering the examples of figures 4a and b and 5a to c, it is well to remember that F_{AB} is a

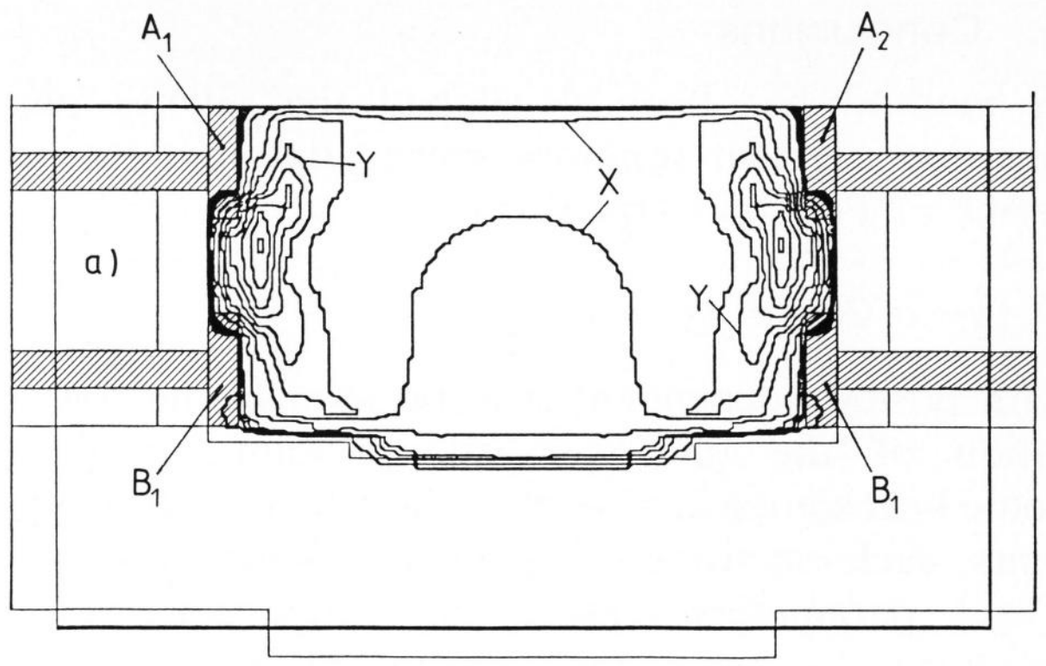

Figures 5a to c. Joule heat contours for an electrically-driven glass melter configuration with a) $F_{AB} = 0$, b) $F_{AB} = +1$, c) $F_{AB} = -1$.

current temporal correlation factor. In the example of figures 4a and b, current temporal correlation $F_{AB} = 0$ will imply voltage temporal correlation $G_{AB} = 0$, as can be seen from equation (39). This occurs because the electrodes of pair B lie on equipotentials from the driving of pair A alone, i.e., $\Delta\phi_{A,B}^{(0)} = 0$, and the electrodes of pair A lie on equipotentials from driving pair B alone, i.e., $\Delta\phi_{B,A}^{(0)} = 0$. In the example of figures 5a to c, by contrast, temporal orthogonality of driving currents ($F_{AB} = 0$) and temporal orthogonality of driving voltages ($G_{AB} = 0$) do not necessarily occur together.

8. Conclusions

A method has been developed that allows two time-independent solutions having different source terms of Poisson's equation

$$\nabla \cdot (-\sigma \nabla \phi) = Q_v$$

with position-dependent σ to be used in the calculation of the time-averaged, position-dependent Joule heat source in a system heated by two electrode pairs, each electrode being a charge source or sink. Three parameters related to average squares or products of either voltages or currents can be set in the calculation using these time-independent solutions and a determining subset of power, rms voltage, or rms current to the two pairs of electrodes. Fairly arbitrary waveforms can be accommodated, subject to the constraint that spatial charge storage effects (capacitive effects) remain small according to the criterion $\varepsilon \omega/\sigma \ll 1$ for angular frequencies ω significantly represented in the Fourier representation and for most spatial points in the region between electrodes. The time-independent potential solutions need to be recalculated only when the conductivity distribution, not the electrical driving, is changed. Extension of this method to more than two electrode pairs is possible. The potential superposition principle can also be applied for electrode systems for which there are no identifiable pairs of electrodes, in which current in at electrode 1 of the pair equals current out at electrode 2. An example of this would be a set of three electrodes connected to the vertices of a three-phase transformer secondary delta configuration. Coupling of the electric model and power density to a three-dimensional computational fluid mechanics code is feasible to investigate thermal patterns and flow of molten glass or soil.

9. Nomenclature

A_1, A_2, B_1, B_2	source (1) or sink (2) region of emf systems A and B, respectively
c	phase angle constant
C	specific heat in J/(kg K)
$d^3 r$	infinitesimal volume element for spatial integration
D	determinant of voltage differences
e	base of natural logarithms = 2.71828 . . .
$\underline{E}$	electric field vector in V/m
$f_A(t), f_B(t)$	time-dependence factor in current source per unit volume for source A or B or associated potential solution, dimensionless
F_{AA}, F_{AB}, F_{BB}	time-averaged products of pairs of time-dependence factors $f_A(t)$ or $f_B(t)$
g_i, g_j	i-th and j-th component, respectively, of gravity vector
G_{AA}, G_{AB}, G_{BB}	time-averaged products of pairs of voltage differences from emf sources A or B in V/m^2
i	$\sqrt{(-1)}$
$I_A^{(0)}, I_B^{(0)}$	source current for reference field A or B
$I_{A,rms}, I_{B,rms}$	root mean square currents associated with emf system A or B in A
J	current density magnitude in A/m^2
$\underline{J}$	current density vector in A/m^2
$\underline{J}^*$	complex conjugate of current density in complex form
J_n	normal component of current density at a surface
k	thermal conductivity in W/(m K)
n	unit normal vector at a surface
p	pressure in Pa
P_A, P_B	time-averaged power from emf system A or B in W
P_v	power per unit volume in W/m^3
$\overline{P}_v$	time-averaged power per unit volume in W/m^3
Q_A, Q_B	current source per unit volume associated with emf source A or B
$Q_A^{(0)}, Q_B^{(0)}$	space-dependence factor in current source per unit volume for source A or B in A/m^3
Q_v	current source per unit volume in A/m^3
$\dot{Q}$	heat generation rate per unit volume in W/m^3
$\underline{r}$	spatial position vector
t	time in s
T	temperature in K
U_i, U_j	i-th and j-th component, respectively, of fluid velocity U in m/s
X_i, X_j	i-th and j-th component, respectively, of position vector
∇	gradient operator
$\nabla \bullet$	divergence operator
Δ	increment of the variable which follows
$\Delta\phi_{A,B}^{(0)}$	potential difference in reference field A between the source and sink electrodes of reference field B
ε	electrical permittivity, dielectric constant times permittivity of vacuum in C^2/(J m)
ϱ	mass density in kg/m^3
ϱ_0	reference mass density in Boussinesq approximation in kg/m^3
ϱ_e	electric charge density in C/m^3
σ	electrical conductivity in A/(V m)
ν	viscosity in kg/(m s)
ϕ	electrical potential in V
$\hat{\phi}$	electrical potential complex amplitude of exp ($i\omega t$) oscillation
ϕ_A, ϕ_B	potential field A or B
$\phi_A^{(0)}(r_{B_2})$	potential in reference field A at the position of electrode 2 of field B
Ψ	additive space-independent field to potential field
ω	angular frequency in rad/s

10. References

[1] Staněk, J.: Electric melting of glass. Amsterdam, Oxford, New York: Elsevier 1977.

[2] Curran, R. L.: Use of mathematical modeling in determining

the effects of electrode configuration on convection currents in an electric glass melter. IEEE Trans. Ind. Appl. **IA-7** (1971) no. 1, p. 116–120.

[3] Curran, R. L.: Mathematical model of an electric glass furnace: Effects of glass color and resistivity. IEEE Trans. Ind. Appl. **IA-9** (1973) no. 3, p. 348–356.

[4] Chen, T.-S.; Goodson, R. E.: Computation of three-dimensional temperature and convective flow profiles for an electric glass furnace. Glass Technol. **13** (1972) no. 6, p. 161–167.

[5] Choudhary, M. K.: Three-dimensional mathematical model for flow and heat transfer in electric glass furnaces. Heat Transfer Eng. **6** (1985) no. 4, p. 55–65.

[6] Choudhary, M. K.: A three-dimensional mathematical model for flow and heat transfer in electrical glass furnaces. IEEE Trans. Ind. Appl. **IA-22** (1986) no. 5, p. 912–921.

[7] Ungan, A.; Viskanta, R.: Identification of the structure of the three dimensional flow in an idling container glass melter. Glass Technol. **28** (1987) no. 6, p. 252–260.

[8] Ghandakly, A. A.; Curran, R. L.: Accurate modeling of interelectrode resistance and power dissipation in electric glass melters. IEEE Trans. Ind. Appl. **24** (1987) no. 6, p. 1057–1061.

[9] Tiwary, R.; Stickler, D. B.; Woodroffe, J.: Numerical modeling to support engineering development of an advanced glass melter. Am. Ceram. Soc. Bull. **67** (1988) no. 11, p. 1791–1796.

[10] Horvath, Z.; Hilbig, G.: Mathematical model for fuel-heated glass melting tanks. Glastech. Ber. **61** (1988) no. 10, p. 277–282.

[11] Murnane, R. A.; Johnson, W. W.; Moreland, N. J.: The analysis of glass melting processes using three-dimensional finite elements. Int. J. Numer. Methods Fluids **8** (1988) no. 12, p. 1491–1511.

[12] Brouns, R. A.; Timmerman, C. L.: In situ thermoelectric stabilization of radioactive wastes. In: Post, R. P. (ed.): Proceedings of the Symposium on Waste Management 82, Tucson, AZ (USA) 1982. Univ. Arizona, College of Engineering, Tucson 1982. p. 449–463.

[13] Buelt, J. L.; Timmerman, C. L.; Oma, K. H. et al.: In situ vitrification of transuranic waste II – An updated systems evaluation and applications assessment. PNL-4800. Suppl. 1. Richland, WA: Pacific Northwest Laboratory 1987.

[14] Trent, D. S.; Eyler, L. L.; Budden, M. J.: TEMPEST. A three-dimensional time-dependent computer program for thermal hydraulic analysis. PNL-4348. Rev. 1. Richland, WA: Pacific Northwest Laboratory 1985.

[15] Trent, D. S.; Eyler, L. L.: TEMPEST. A three-dimensional time-dependent computer program for hydrothermal analysis. Vol. 1. Numerical methods and input instructions. PNL-4348. Rev. 2. Richland, WA: Pacific Northwest Laboratory 1989.

[16] Eyler, L. L.; Skarda, R. J.; Crowder, R. S. et al.: Physical and numerical modeling of Joule-heated melters. PNL-5491. Richland, WA: Pacific Northwest Laboratory 1985.

91R0273